


# AUSTEMPERED DUCTILE IRON WITH DUAL MICROSTRUCTURES: EFFECT OF INITIAL MICROSTRUCTURE ON THE AUSTENITIZING PROCESS

**Wilson Luiz Guesser** 

Santa Catarina State University, Joinville, SC, Brazil  
Foundry Consultant at Tupy Foundry, Joinville, SC, Brazil

**Clarissa L. Lopes**

UNISOCIESC, Rua Albano Schmidt, 3333, Joinville, SC 89206-001, Brazil

**Pedro A. N. Bernardini**

Santa Catarina Federal University, Florianópolis, SC, Brazil

Copyright © 2020 American Foundry Society  
<https://doi.org/10.1007/s40962-019-00397-y>

## Abstract

*This work compares alternatives for the production of high ductility ADI, austempered from an intercritical austenitizing temperature range, with a microstructure of ferrite + ausferrite. Different initial microstructures were selected, including ferrite, pearlite, pearlite + ferrite, martensite and ausferrite. The samples were austenitized within the intercritical zone (795 °C) for different times (up to 12 h) and then austempered at 350 °C. The evolution of the formation and distribution of ferrite and austenite during the austenitizing process for the different initial microstructures was studied. For the selected austenitizing temperature, all of the initial microstructures produced 30% ferrite (70% ausferrite) in the final microstructure (after 12 h). The mechanical properties depend upon the distribution and refinement of the ferrite and ausferrite areas. Spheroidized carbides from pearlite are not completely dissolved during intercritical austenitizing for 2 h. Graphite nodules are an important source of carbon for the*

*austenite formed from starting microstructures of ferrite, pearlite + ferrite and pearlite with grain boundaries being the main pathway for carbon diffusion. Austenitizing started away from the graphite nodules at eutectic cell boundaries due to Si segregation. For starting microstructures of ferrite, pearlite and pearlite + ferrite, a homogeneous distribution of austenite does not occur. Rather, it is concentrated on eutectic cell boundaries and ferrite grain boundaries with large areas of ferrite around the graphite nodules. For starting microstructures of martensite and ausferrite, carbon is evenly distributed and quickly dissolved, resulting in a homogeneous distribution of austenite and ferrite with the best combination of strength and ductility.*

**Keywords:** ADI, mechanical properties, intercritical ADI

## Introduction

High ductility ADI parts in grades 750-500-11 (ASTM A897M/16) or 800-500-10 (ISO 17804/2005) can be produced using high austempering temperatures, or alternatively designed with a microstructure of ausferrite + ferrite, utilizing an intercritical austenitizing

treatment, followed by austempering. This grade of ADI brings the opportunity of reducing the weight of automotive parts by replacing ferritic ductile iron as this material combines ductility and high strength. For example, suspension parts can be redesigned using this combination of properties.

The distribution of ferrite is completely different in intercritical ADI compared to ferrite/pearlite ductile irons. The

---

This paper is an invited submission to IJMC selected from presentations at the 2nd Carl Loper 2019 Cast Iron Symposium held September 30 to October 1, 2019, in Bilbao, Spain.

bull's-eye distribution of ferrite concentrates deformation in the ferrite near graphite nodules, promoting the initiation of cracks in these areas.<sup>1</sup> In intercritical ADI, the ferrite distribution is not concentrated solely near graphite nodules so this microstructure offers more resistance to crack initiation.<sup>2</sup> The results are high strength together with high elongation in intercritical ADI.<sup>3-5</sup>

On the other hand, the low austenitizing temperature presents some challenges for this treatment. Dissolving carbides from pearlite is a slow process at these temperatures,<sup>6</sup> and carbon diffusion from the graphite nodules occurs mainly through grain boundaries. Segregation of substitutional alloying elements during solidification,<sup>7</sup> mainly those elements that dictate the position of austenite + ferrite field, can affect the distribution of austenite and ferrite.<sup>8</sup> The inverse segregation of silicon seems to be the most important factor on the local austenitizing temperatures.<sup>6</sup> These limitations for homogenization show that the initial microstructure can affect the final microstructure, and, subsequently, the mechanical properties.

As a result, this work focuses on studying the effect of different starting microstructures on austenitizing and on the final mechanical properties that were obtained.

## Experimental Procedures

The melt was produced in an induction furnace with the composition listed in Table 1. Y-blocks (25 mm, 1-in) were cast in chemically bonded sands. For the composition in Table 1, the upper and lower critical temperatures are 841 and 775 °C, respectively.<sup>9</sup> Different initial microstructures were produced by heat treatment processes according to Table 2. Table 3 and Figure 1 show the microstructures that were produced: ferrite, pearlite, pearlite + ferrite (as-cast), ausferrite, and martensite.

The samples were austenitized in a salt bath at 795 °C to produce a microstructure with 30% ferrite and 70% austenite<sup>4</sup> and maintained for 2, 6 and 12 h at this temperature, to study the phase transformation kinetics. Austempering, in a salt bath, at 350 °C for 2 h was followed.

**Table 1. Chemical Composition of the Samples (%)**

C	Si	Mn	Ni	Mo	Cu	S	Mg
3.58	2.71	0.20	0.92	0.14	0.56	0.017	0.040

**Table 2. Heat Treatment Processes Used to Produce Different Initial Microstructures**

Microstructure	Heat treatment
Ferrite	900 °C for 2 h, cooling in the furnace to 700 °C, holding for 20 h, air cooling
Pearlite	900 °C for 2 h, cooling with forced air
As-cast	—
Martensite	900 °C for 2 h, cooling in oil, tempered at 160 °C for 2 h
Ausferrite	900 °C for 2 h, 360 °C for 2 h

**Table 3. Initial Microstructures**

	Matrix	Nodularity (%)	Nod/mm <sup>2</sup>	Hardness (HB)
Ferrite	100% ferrite	93	212	157
Pearlite	100% pearlite	97	206	286
As-cast	50% pearlite	96	223	184
Martensite	100% tempered martensite	94	235	433
Ausferrite	100% ausferrite	92	193	292

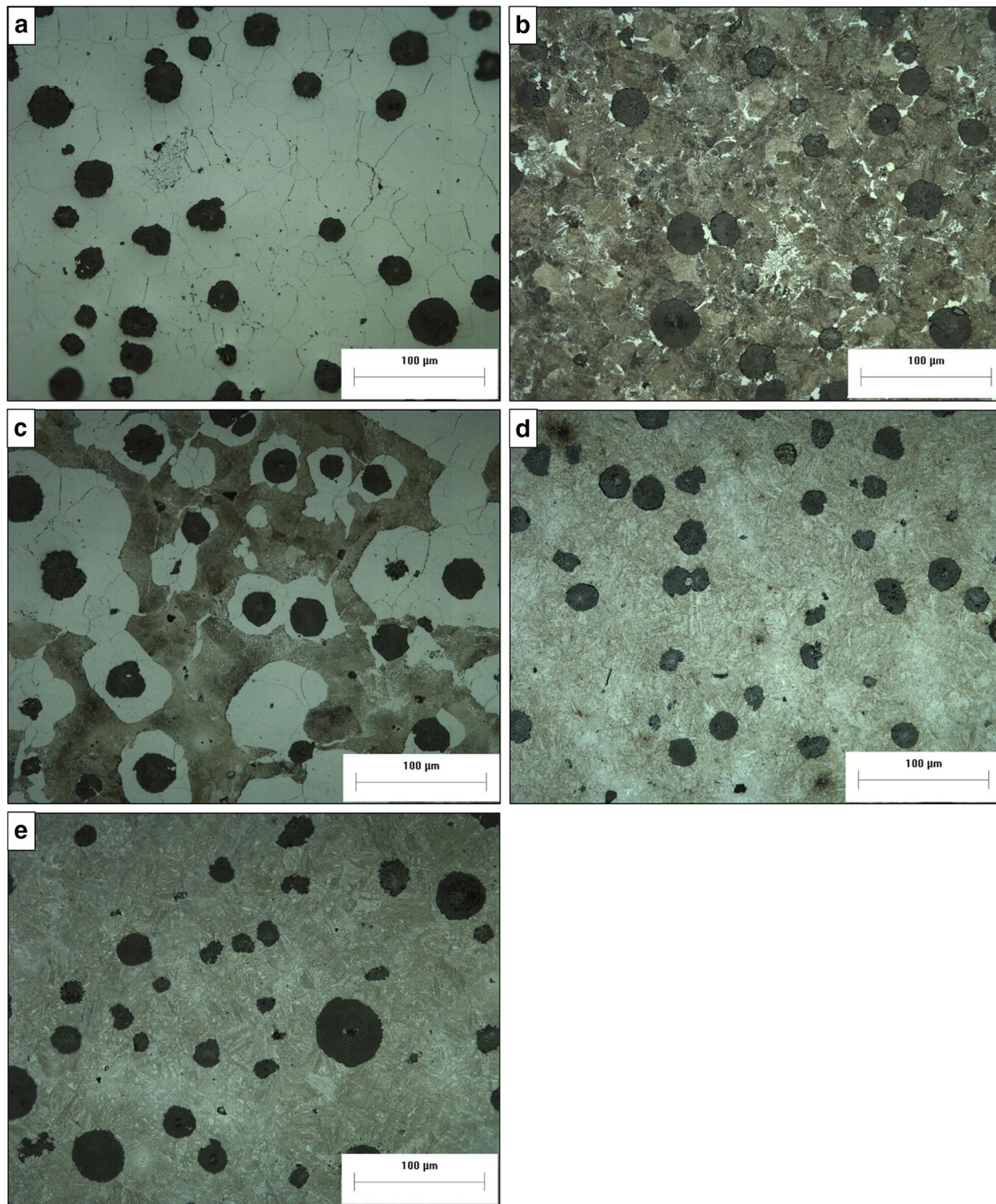


**Figure 1. Different starting microstructures to study the transformation kinetics during austenitizing: (a) ferrite, (b) pearlite, (c) as-cast ferrite + pearlite, (d) martensite, (e) ausferrite.**

Tensile tests were performed according to ISO 6892. The Quality Index was also calculated (Eqn. 1), which compares the distance of the results from the line defining the

minimum mechanical property values from the ASTM Standard for ADI (A897/16), according to a procedure developed before for pearlitic ductile irons.<sup>10</sup>

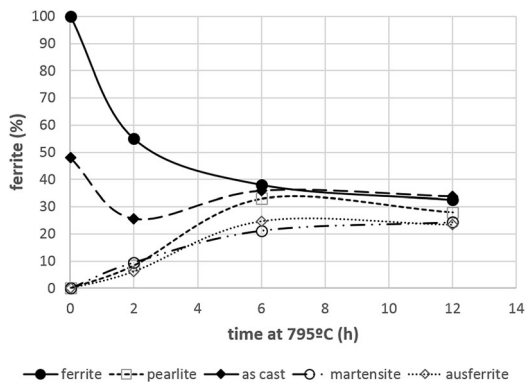


**Figure 2. Ferrite percentage with austenitizing time for different starting microstructures. Intercritical austenitizing at 795 °C was used.**

$$\text{Quality Index} = 0.068 \times \text{UTS} + 4.44 \times \text{Elong}$$

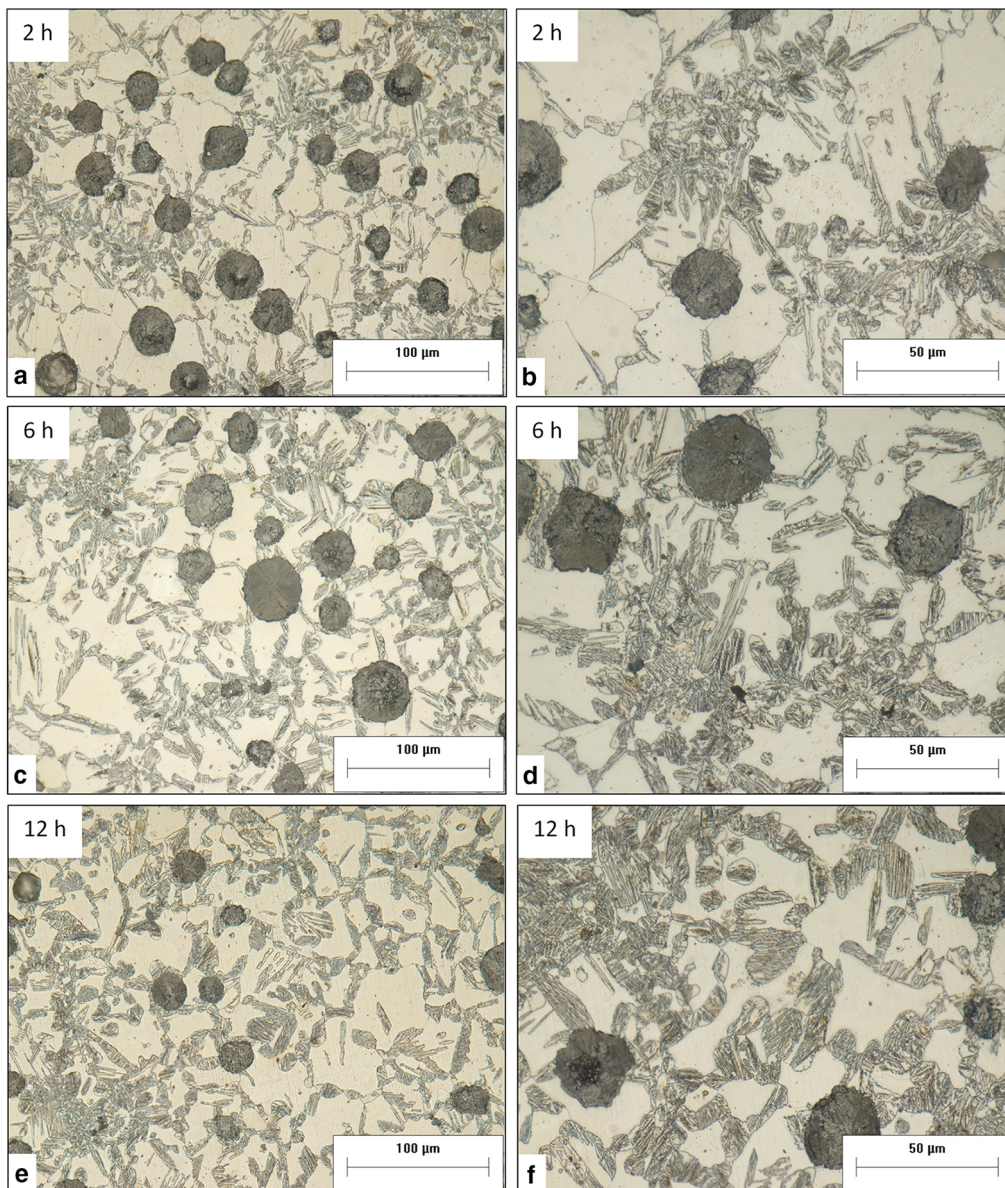
Eqn. 1

For example, a value of QI = 120% means that the results are 20% higher than the minimum established by ASTM Standard A897.

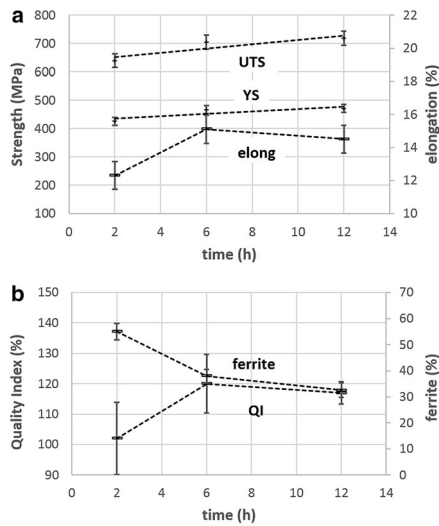
Further details of the experimental procedures can be found elsewhere.<sup>11</sup>

## Results and Discussion

Figure 2 shows the ferrite evolution during austenitizing at 795 °C for the various initial microstructures. With starting



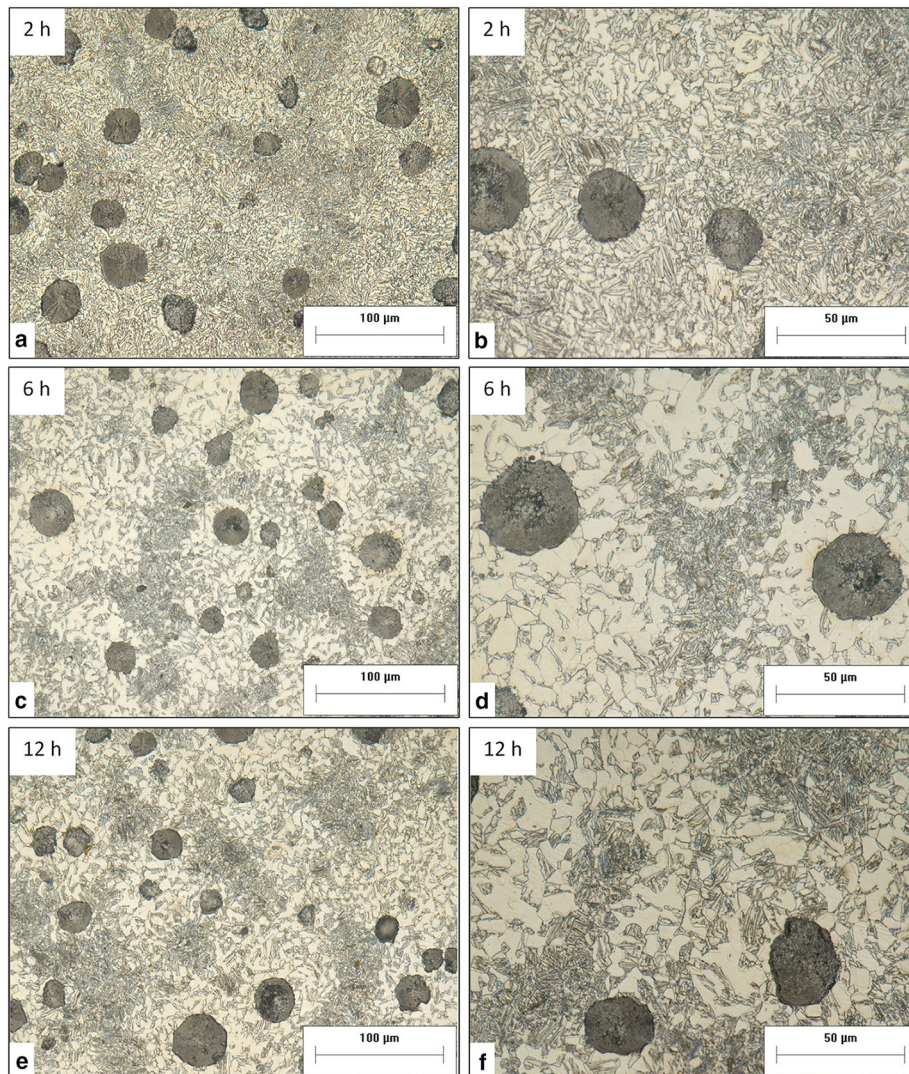
**Figure 3. Microstructure evolution at 795 °C when austenitizing samples with an initial ferrite starting matrix: (a, b) 2 h. (c, d) 6 h. (e, f) 12 h.**



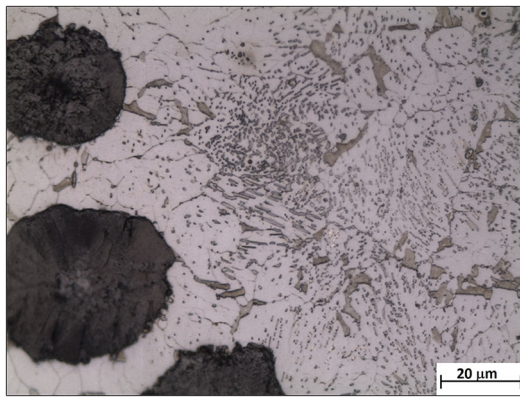
**Figure 4. (a) Effect of austenitizing time at 795 °C on the mechanical properties and (b) on the Quality Index for an initial ferritic microstructure austempered for 2 h at 350 °C.**

microstructures of ferrite and pearlite + ferrite, there is a decrease in the ferrite content with the treatment. With initial microstructures of pearlite, martensite and ausferrite, the ferrite content increases with time. All of the final microstructures had approximately 30% ferrite.

Starting with a ferrite matrix (Figure 3), the only source of carbon for the austenite is the graphite nodules. Austenitizing starts at cell boundaries, mainly due to Si segregation, leaving large areas of ferrite around graphite nodules (Figure 3a). The formation of austenite follows near ferrite grain boundaries. The final distribution of ferrite is concentrated around graphite nodules, but partitioned by austenite formed at grain boundaries. After 12 h, there are many ferrite areas near the graphite nodules, with a size of 30–50 μm.



**Figure 5. Microstructure evolution at 795 °C when austenitizing samples with an initial pearlite-starting matrix: (a, b) 2 h. (c, d) 6 h. (e, f) 12 h.**



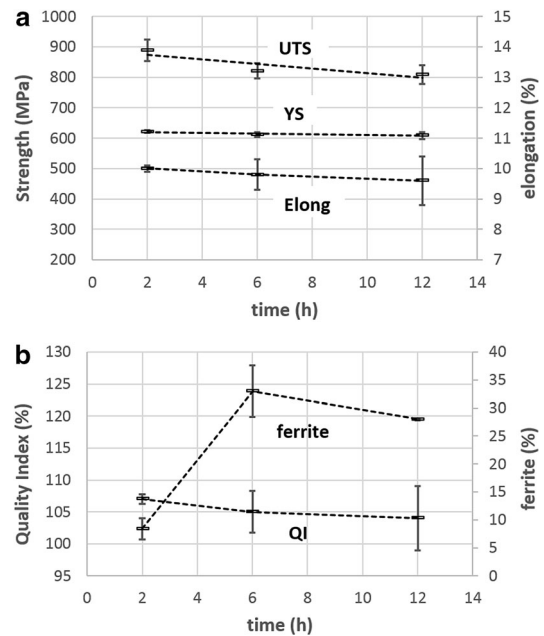
**Figure 6. Spheroidized carbides formed at cell boundaries for an initial pearlite-starting matrix held for 2 h at 795 °C.**

Figure 4 shows the effect of the austenitizing time on the mechanical properties after austempering. The strength increases because of decreasing ferrite content. At the same time, the elongation increases caused by the change in the ferrite morphology being distributed more homogeneously. The Quality Index can reach values close to 120%.

Figure 5 shows the microstructure evolution starting with a pearlitic matrix. In this case, two processes occur simultaneously: ferrite and austenite formation. Their development depends on carbon diffusion from pearlite away from the ferrite into the austenite and into the graphite nodules. With 6 h at 795 °C, the microstructure shows an increase in ferrite areas near the graphite nodules. It follows the austenitizing near ferrite grain boundaries.

The result is a fine distribution of ferrite and austenite. The decomposition of pearlitic carbides takes some time, and it is possible to observe some intercellular areas with spheroidized carbides with 2 h at 795 °C (Figure 6). After 12 h, austenite is mainly concentrated at the eutectic cell boundaries (Figure 5). The size of ferrite areas near the graphite nodules is 10–15 μm. The slow decomposition rate of carbides from pearlite and the final distribution of austenite follow the segregation of silicon during solidification.

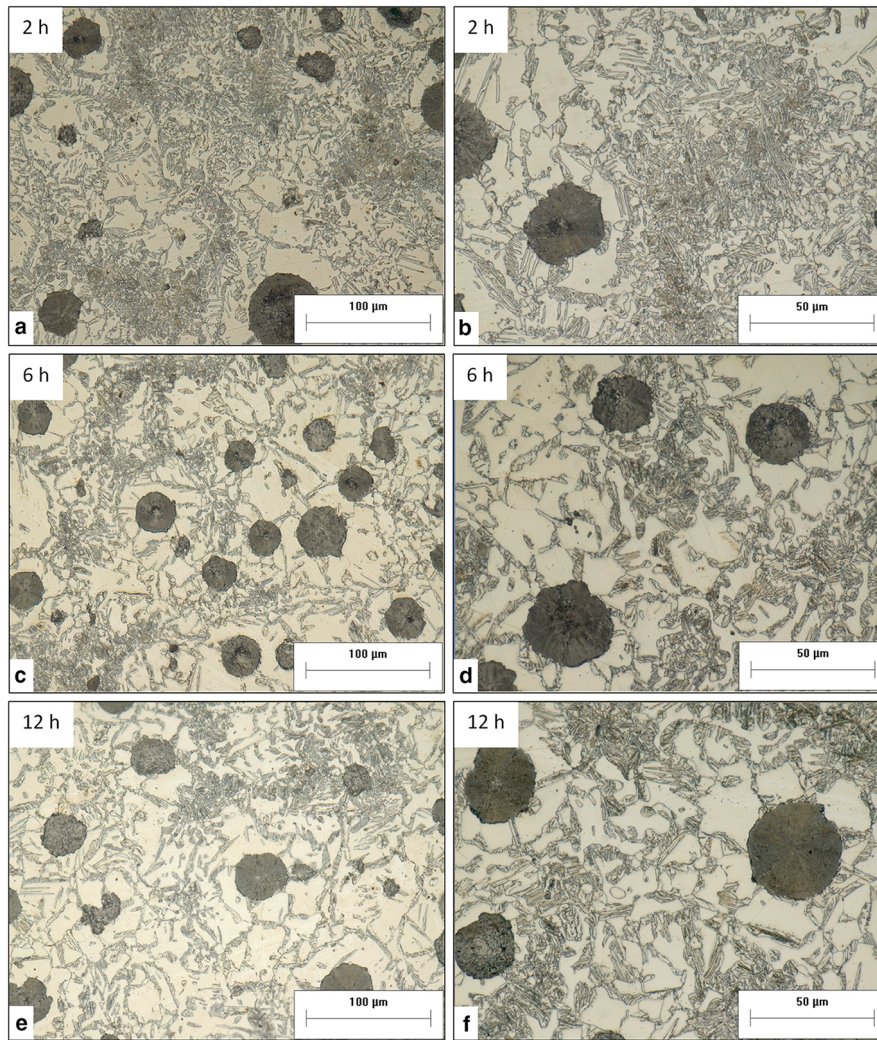
Figure 7 shows the effect of austenitizing time on the mechanical properties for an initial starting microstructure of pearlite. The small decrease in strength is a result of the increased amount of ferrite in the microstructure with the time. The Quality Index is relatively low with values around 105%.



**Figure 7. (a) Effect of austenitizing time at 795 °C on the mechanical properties and (b) on the Quality Index for an initial pearlite-starting microstructure austempered for 2 h at 350 °C.**

Figure 8 presents the microstructure evolution when austenitizing samples with an as-cast pearlite + ferrite starting microstructure with 50% ferrite. The austenitizing process starts at the eutectic cell boundaries, far from the graphite nodules, and along ferrite grain boundaries. With 2 h at 795 °C, one can see that ferrite is concentrated around graphite nodules, forming large areas of ferrite. After 12 h, this is still the predominant microstructure, but with smaller areas of ferrite divided by austenite that formed along the grain boundaries. Ferrite areas near the graphite nodules are within the size of 25–30 μm. At the same time, areas of undissolved pearlite, at eutectic cell boundaries, can still be seen after 2 h of treatment as also reported by Franco et al.<sup>12</sup> With longer times, all pearlite is dissolved.

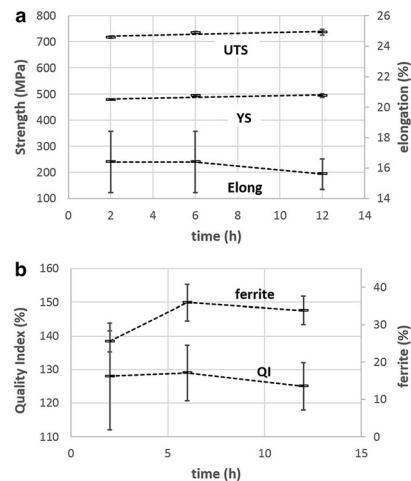
Figure 9 presents the effect of austenitizing time on the mechanical properties, for an as-cast pearlite + ferrite starting microstructure. From 2 h to 12 h of treatment, the changes in mechanical properties are small, reflecting the small changes in microstructure (Figure 8). Even if the microstructure changes are small, the strength values improved with time, reflecting the formation of austenite (ausferrite) near the graphite nodules. Quality Index values are in the range of 125–130%.



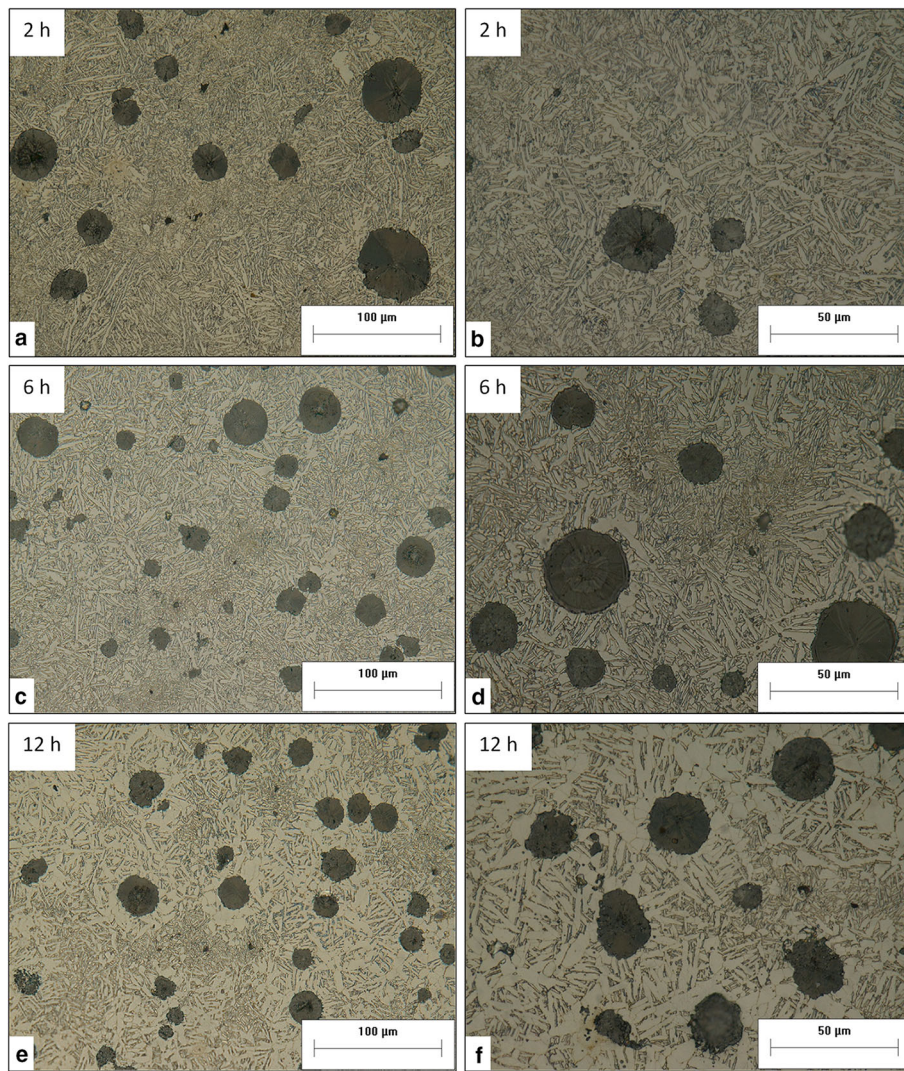
**Figure 8. Microstructure evolution when austenitizing samples with an as-cast pearlite + ferrite starting microstructure with 50% ferrite: (a, b) 2 h. (c, d) 6 h. (e, f) 12 h.**

Figure 10 shows the microstructure evolution with martensite as the initial microstructure. In this case, carbon is homogeneously distributed in the matrix. Ferrite forms in an acicular shape. With 2 h at 795 °C, it is possible to observe the formation of secondary graphite particles (Figure 11). Even if the eutectic cell boundaries present only austenite, the distribution of ferrite and austenite can be considered fine and almost homogeneous (Figure 10). The size of ferrite areas near the graphite nodules is 10–15 μm after 6 h treatment and 30–40 μm after 12 h at 750 °C.

Figure 12 presents the evolution of mechanical properties with the austenitizing time for an initial starting matrix of martensite. The strength decreases with time due to an increase in the ferrite content. The decrease in elongation after 6 h is caused by the presence of secondary graphite, promoting a large number of ductile microvoids during



**Figure 9. (a) Effect of austenitizing time at 795 °C on the mechanical properties and (b) on the Quality Index for an initial starting as-cast pearlite + ferrite microstructure austempered for 2 h at 350 °C.**



**Figure 10. Microstructure evolution at 795 °C with martensite as the initial starting matrix. (a, b) 2 h. (c, d) 6 h. (e, f) 12 h.**

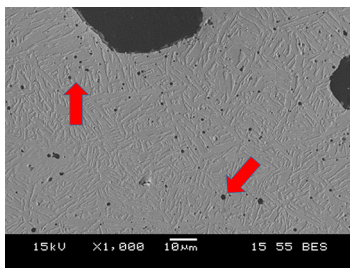


**Figure 11. Secondary graphite formation at 795 °C from the initial martensite matrix after 2 h of treatment.**

tensile testing.<sup>13</sup> The Quality Index for 6 h at 795 °C shows values near 130%. For this initial microstructure, longer times than 6 h should be avoided due to secondary graphite formation and increased size of ferrite areas near the graphite nodules.

Figure 13 presents the austenitizing process starting from an ausferrite initial matrix. Ferrite forms in an acicular shape. In addition, the carbon distribution is homogeneous with resulting microstructures of fine areas of ferrite and austenite. The size of the ferrite areas near graphite nodules



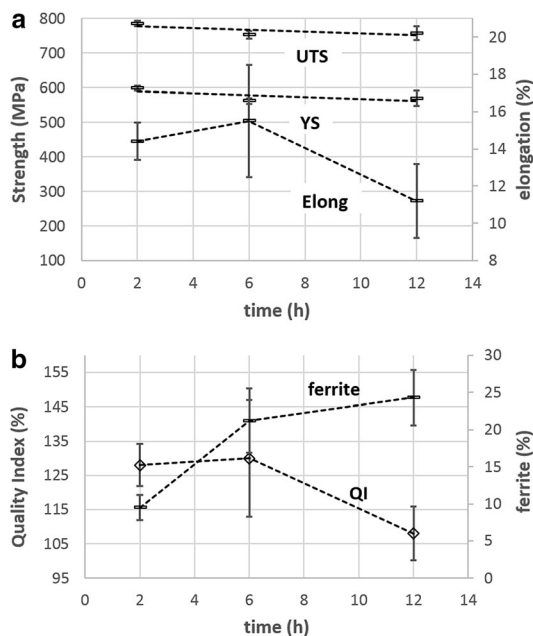


**Figure 12. (a) Effect of austenitizing time at 795 °C on the mechanical properties and (b) on Quality Index for an initial starting matrix of martensite for samples austempered for 2 h at 350 °C.**

is 5–10  $\mu\text{m}$  after 6 h treatment, and 10–20  $\mu\text{m}$  after 12 h at 795 °C.

Figure 14 shows the effect of austenitizing time on the mechanical properties of samples austempered at 350 °C for a starting matrix of ausferrite. The small decrease in the strength and increase in elongation are a result of increasing the amount of ferrite with time. The Quality Index reaches values around 145% with 6 h of austenitizing; higher times should be avoided due to the increased size of ferrite areas near the graphite nodules.

Figure 15 presents the best mechanical properties results for each initial microstructure along with the austenitizing time for each case. A line with the minimum values of

ASTM Standard A897/2006 for ADI is also included. The distance of a point to the line represents the Quality Index. Ferrite, as-cast pearlite + ferrite and martensite have similar Quality Index values (120–130%), while pearlite has a Quality Index of 107%. The reason for this lower Quality Index is not clear for the pearlite initial microstructure. An initial microstructure of ausferrite provides the highest Quality Index (144%) because of a fine distribution of ferrite and austenite (ausferrite).

## Conclusions

The distribution and morphology of ferrite and austenite during intercritical austenitizing are determined by the initial microstructure and by the segregation profile of alloying elements, mainly Si. Austenite formation starts at eutectic cell boundaries and in a second stage near ferritic grain boundaries around graphite nodules. On the other hand, there is a trend for ferrite formation near graphite nodules. Depending on the starting microstructure, ferrite content can increase (pearlite, martensite, ausferrite starting matrix) or decrease (ferrite or ferrite predominant matrix). Ferrite-rich initial microstructures result in large areas of ferrite near the graphite nodules. Acicular initial microstructures result in the formation of acicular ferrite, with a very fine distribution of austenite and ferrite.

With martensite as the starting microstructure, there is a trend to precipitate secondary graphite particles during intercritical austenitizing which can lead to a reduction in elongation.

In pearlite initial microstructures, primarily in alloyed cast irons, spheroidized carbides from pearlite at cell boundaries can survive for more than 2 h at intercritical temperatures.

Ausferrite initial microstructures resulted in a very fine distribution of ferrite and austenite, with the best mechanical properties of the tested materials.

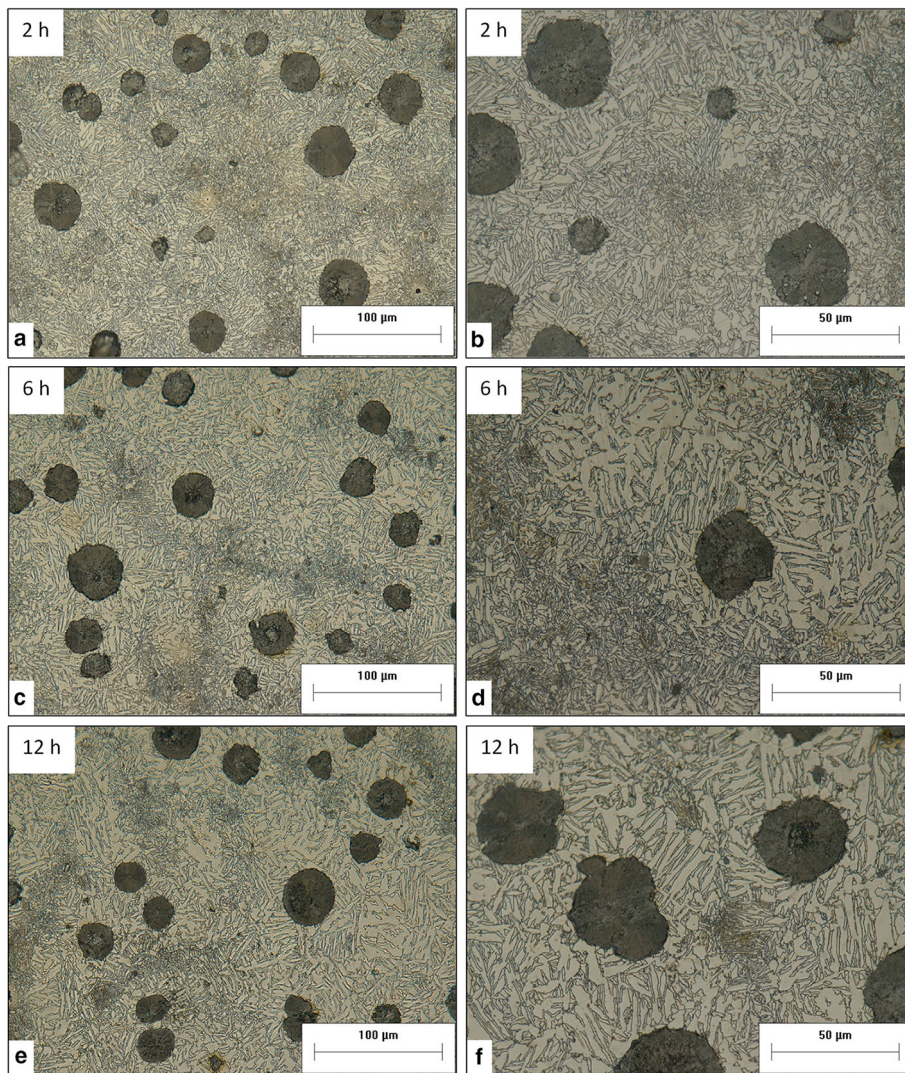


**Figure 13.** Austenitizing process starting from ausferrite as initial starting matrix. (a, b) 2 h. (c, d) 6 h. (e, f) 12 h.

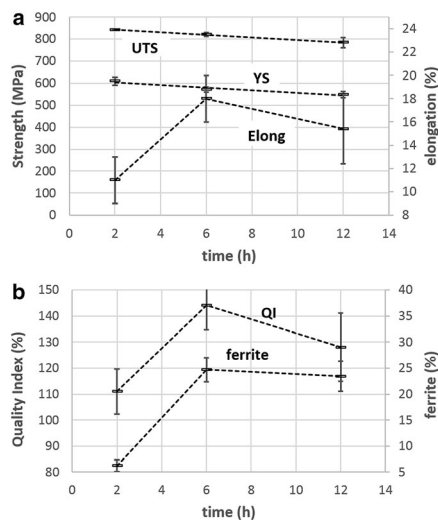


**Figure 14. (a) Effect of austenitizing time at 795 °C on the mechanical properties and (b) on Quality Index for an initial starting microstructure of ausferrite austempered for 2 h at 350 °C.**

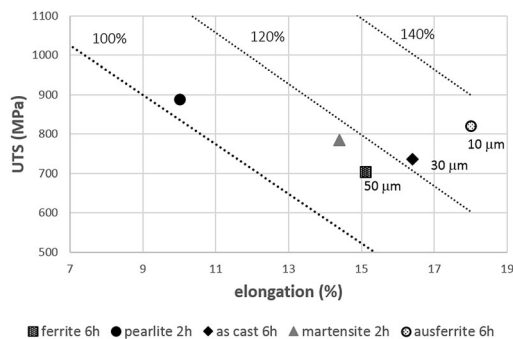


**Figure 15. Summary of the best mechanical properties for each starting microstructure. Each line represents a Quality Index or the distance from the minimum values of ASTM Standard A897/2006 for ADI. The ferrite size ( $\mu\text{m}$ ) near graphite nodules is provided for some of the microstructures.**

## Acknowledgements

The experiments reported in this paper were conducted in partnership with Tupy Foundry and Santa Catarina Federal University—UFSC.

## REFERENCES

1. W.L. Guesser, L.C. Guedes, R.R. Vieira, The influence of hydrogen on the fracture mechanism and mechanical properties of blackheart malleable and

ductile irons, in *59th World Foundry Congress* (São Paulo, 1992), pp. 22.4–22.11

2. H. Santos, Mecanismos de fratura de ferro nodular austemperado a partir da zona crítica. Master Thesis, UDESC, (Brasil, 2010)
3. D. Rousiere, J. Aranzabal, Development of mixed (ferrite–ausferitic) structures for spheroidal graphite irons. *Metall. Sci. Metall.* **18**(11), 24–29 (2000)
4. W.L. Guesser, E. Franco, C. Lussoli, C.E. Costa, Ferro nodular austemperado a partir da zona crítica, in *14th Anual Foundry Congress ABM-ABIFA*, (São Paulo, 2009)
5. M. Erdogan, V. Kilicli, B. Demir, Transformation characteristics of ductile iron austempered from intercritical austenitizing temperature ranges. *J. Mater. Sci.* **44**(5), 1394–1403 (2009)
6. E. Franco, C.E. Costa, W.L. Guesser, Estudo dos parâmetros de austenitização para fabricação do ferro nodular austemperado usinável, in *8th Congreso Iberoamericano de Ingeniería Mecânica* (Cusco Perú, 2007)
7. G. Jolley, Segregation in nodular iron and its influence on mechanical properties. *Br. Foundrym.* **3**, 79–92 (1967)
8. C.L. Lopes, Estudo da influência das temperaturas de austenitização nas propriedades mecânicas do ferro nodular austemperado a partir da zona crítica. Master Thesis, UDESC, (Brasil, 2009)
9. R. Hummer, W. Westerholt, Untersuchungen zur Wärmebehandlung von Gusseisen mit Kugelgraphit unter besonderer Berücksichtigung der Herstellung von GGG-50. *Giesserei-Praxis*, 1979, no 1/2, pp. 15–20
10. W.L. Guesser, E. Melleras, C. Cabezas, I. Masiero, Avaliação da qualidade metalúrgica em ferros fundidos nodulares e cinzentos, in *15th CONAF and BRICS Forum*, ABIFA, (São Paulo, 2011)
11. C.L. Lopes, Estudo da influência da microestrutura na cinética de austenitização na zona crítica e propriedades mecânicas de ferros nodulares austemperados duais. *PhD Thesis*, UFSC, (Brasil, 2014)
12. E. Franco, C.E. Costa, J. Stahlschmidt, W.L. Guesser, Otimização dos parâmetros de austenitização de um ferro nodular austemperado a partir da zona crítica. *Tecnol. Metal. Mater. Miner.* **6**(3), 142–146 (2010). <https://doi.org/10.4322/tmm.00603004>
13. W.L. Guesser, Fragilização por hidrogênio em ferros fundidos nodulares e maleáveis pretos. PhD Thesis, USP, (São Paulo, 1993). <http://www.teses.usp.br/teses/disponiveis/3/3133/tde-04092019-141731/>. Accessed 26 June 2019

**Publisher's Note** Springer Nature remains neutral with regard to jurisdictional claims in published maps and institutional affiliations.